POLITECNICO DI TORINO
Repository ISTITUZIONALE

Thermal buckling of variable stiffness composite laminates using high order plate finite elements

Original
Thermal buckling of variable stiffness composite laminates using high order plate finite elements / Bracaglia, F., Masia, R., Pagani, A., Zappino, E., Carrera, E.. - In: COMPOSITE STRUCTURES. - ISSN 0263-8223. - 345:(2024). [10.1016/j.compstruct.2024.118393]

Availability:
This version is available at: 11583/2992900 since: 2024-09-30T07:48:13Z

Publisher:
Elsevier

Published
DOI:10.1016/j.compstruct.2024.118393

Terms of use:

This article is made available under terms and conditions as specified in the corresponding bibliographic description in the repository

Publisher copyright

(Article begins on next page)

08 June 2026

Composite Structures 345 (2024) 118393

Contents lists available at ScienceDirect

Composite Structures

journal homepage: www.elsevier.com/locate/compstruct

Thermal buckling of variable stiffness composite laminates using high order plate finite elements

F. Bracaglia, R. Masia, A. Pagani *, E. Zappino, E. Carrera

Mul2 Lab, Department of Mechanical and Aerospace Engineering, Politecnico di Torino, Corso Duca degli Abruzzi 24, 10129 Torino, Italy

ARTICLE INFO

Keywords:
Variable angle tow
High-order theories
FEM
Buckling
Thermal analysis

ABSTRACT

This paper proposes a study on the thermal buckling of Variable Angle Tow (VAT) composite plates using high-order theories. Here, the governing equations are derived via the principle of virtual work. Under the assumption of linear pre-buckling, the stability problem is reduced to a linear eigenvalue analysis considering proportional geometric stiffness. In contrast, a constant thermal load is assumed to be known along the plate thickness, and the uncoupled thermo-mechanical formulation is used, where the thermal effects are described as external loads. The plate is discretized using the Finite Element Method (FEM) and high-order theories are developed using the Carrera Unified Formulation (CUF). Using the CUF, the equations are expressed as an invariant of the plate theory approximation order. Therefore, Equivalent Single Layer (ESL) and Layer-Wise (LW) models can be easily implemented. Several geometries and lamination cases are considered for verification purposes, including different side-to-thickness ratios and fiber orientations, which result in various anisotropy effects. In addition, the effect of changing constraints and materials is evaluated. Particular attention is paid to the effect of the structural theory approximation on the evaluation of the thermal buckling load. It is shown that the correct evaluation is highly dependent on the edge-to-thickness ratio and on the anisotropy given by both the fiber orientation and the material properties. As a final remark, sensitivity analysis and best fiber angle solutions are discussed to highlight the importance of the LW modeling approach.

1. Introduction

Over the years, composite materials have attracted increasing interest in different industries, including aerospace, automotive, mechanic, and civil engineering, particularly due to their high strength-to-weight and stiffness-to-weight ratio [1,2]. These materials offer not only reduced weight but also valuable properties, including an interesting thermal application range. The thermal properties, which can be customized through fiber orientation, coupled with the possibility of negative coefficients of thermal expansion, support the use of composite materials for specific thermal applications [3]. Moreover, their ability to tailor directional stiffness and strength makes it possible to create large and complex-shaped components in a single part without additional connections [4]. This tailoring capability is even more present in Variable Angle Tows (VAT) composite materials that are different from traditional composites due to the characteristic curved fibers.

VATs are advanced composite materials exhibiting a local variation in the material properties. The idea of curved deposition is not new but has become achievable only in the last few years due to technological gains. VATs were deeply described by Hyer and Charette in 1991 [5] when new technologies for fiber deposition were developed. In the VAT framework, it is possible to act on more degrees of freedom than traditional composites to adapt the material deposition to loads, boundary conditions, and geometric configurations in order to select the best fiber orientation distribution. The VAT capability to adapt fiber deposition has been widely researched over the last few years. The most frequently studied areas are the optimal fiber deposition to reinforce hole geometries [6,7] and optimize the critical buckling load [8–10].

Buckling is a non-linear phenomenon associated with a sudden change in the shape of the thin structure. The associated displacement is typically very pronounced and can occur smoothly without causing permanent damage or can occur abruptly with catastrophic outcomes. In the case of flat panels, when buckling starts, failure does not occur necessarily [11]. Nevertheless, the buckled deformed shape influences the structural behavior and this phenomenon can be due to various external loads, including thermal ones [12]. Therefore, it is essential to consider thermal buckling in the design for a safe and lightweight structure when thermal loading may be present.

* Corresponding author.
E-mail addresses: francesca.bracaglia@polito.it (F. Bracaglia), rebecca.masia@polito.it (R. Masia), alfonso.pagani@polito.it (A. Pagani), enrico.zappino@polito.it (E. Zappino), erasmo.carrera@polito.it (E. Carrera).

https://doi.org/10.1016/j.compstruct.2024.118393
Received 15 April 2024; Received in revised form 4 July 2024; Accepted 15 July 2024
Available online 20 July 2024
0263-8223/© 2024 The Author(s). Published by Elsevier Ltd. This is an open access article under the CC BY license (http://creativecommons.org/licenses/by/4.0/).

Many thermal buckling studies have been carried out over the years for different configurations [13,14]. To the best of the author knowledge, the study published by Thangaratnam et al. [15] is the first attempt at the Finite Element Method (FEM) application on the thermal buckling of a straight fiber composite plate. In the work, two-dimensional elements are used to investigate the thermal buckling critical load of the plate, and the results are compared to analytical results. After this study, many other analyses were carried out to investigate thermal buckling using FEM. Among those, Shiau et al. [16] focused on the influence of the thermal and mechanical property ratios of the material on the buckling and critical temperature, and Chen et al. [17] employed the thermal-elastic Mindlin plate theory to assess the influence of several parameters on buckling when uniform and nonuniform temperatures are applied. More recently, the thermal-buckling analysis of VAT plates has been studied.

Li et al. [18] presented the buckling thermal analysis for VAT laminate under uniform temperature through the First-order Shear Deformation Theory (FSDT). The influence of different laminations and material parameters on the critical temperature is outlined by Manikam et al. [19] through the use of FEM and FSDT. A thermal-buckling optimization of a symmetric, simply supported VAT plate was examined by Duran et al. [20] and conducted on 4-noded Kirchhoff plate elements. All these studies employed FEM in conjunction with classical theories that were developed for thin and single-layer plates.

The necessity to analyze multilayer structures gives rise to numerous numerical challenges. Consequently, both the description of the in-thickness material properties and the kinematic in-thickness assumptions become central for creating an accurate numerical model. As a consequence, several theories have been introduced to describe the behavior of displacements, strains, and stresses along the thickness considering lamina interfaces. Among these theories, the most widespread are Equivalent Single Layer (ESL) and Layer-Wise (LW) [21]. The ESL considers a homogenization of the material properties along the thickness, analyzing a one-layer plate with equivalent properties. Conversely, the LW model considers each layer individually and imposes continuity conditions at each interface. For the latter issue, high-order theories are introduced. Even though classical theories, such as the Kirchhoff theory or FSDT, are appropriate for a wide range of applications, some high-order phenomena cannot be captured through classical theories [22]. High-order theories allow the accurate calculation of the stresses rising along the whole plate with more precise results, enabling the consideration of the phenomena due to the high anisotropy of these materials. Furthermore, the importance of considering the transverse shear strains in thermal problems is also demonstrated through the use of modified FSDT in [23,24] for functionally graded material. Due to the high complexity of VAT, some works on non-linear thermal analyses for post-buckling and large deflections of VAT have been published recently [25–27].

The need to use high-order models to describe VAT behavior, also in case of mechanical problems, is demonstrated in [28,29] where the Carrera Unified Formulation (CUF) is employed to implement high kinematic models that allow the consideration of the shear deformation in the problem solution. The CUF is also used in conjunction with the Ritz method by Vescovini et al. [30] that described the thermal buckling of VAT employing refined theories.

The CUF is a unified framework that can be used to derive any FEM model for any structural element with the use of Fundamental Nuclei. These FNs are the fundamental components of the matrices that describe the structural problem and are independent of the selected kinematic theory. Furthermore, the formulation makes a multifield load easy to implement, and the study of multilayered structures is possible [31] thanks to the potentially unlimited degree of freedom that can be imposed at each node. The present work exploits the CUF within the FEM method to investigate the critical thermal buckling load of a VAT plate through high-order theories.

The present work aims to assess the influence of the adopted high-order theory on the evaluation of the buckling critical temperature within the Finite Element framework in a more general form using high-order theories. The use of CUF demonstrates that a model with high-order theories combined with the FEM is mandatory to obtain a realistic description of the phenomenon. Furthermore, thanks to the use of FEM, it is possible to describe a wide range of constraints. In contrast, the widespread use of 2D classical models includes some limitations in terms of constraints and an inability to accurately represent phenomena where the volumetric part has a significant effect.

The manuscript is organized in the following sections. First, Section 2 describes the numerical approach used to describe the VAT. In Section 3.1, the Carrera Unified Formulation used with the Finite Element Method is reported, and the governing equations for the linearized thermal buckling problem are obtained in Section 3.2. The numerical results are reported in Section 4, where different geometries, materials, and constraints are evaluated. Finally, some conclusions are outlined in Section 5.

2. Varibale angle tow plates

Variable Angle Tow (VAT) composite materials exhibit a distinctive curved fiber deposition, resulting in an increased degree of freedom for lamina customization. Traditional composite materials have been extensively researched across a wide range of applications, and incorporating additional degrees of freedom in the deposition process offers novel advantages. The curved fiber path enables the adaptation of fiber orientation in response to external loads or specific phenomena that need to be mitigated.

The variation in fiber orientation within the lamina plane can be described using various mathematical models. Among these, in the present work, the deposition is described by linear variation along a specific direction within the plane of the lamina. In this context, the local deposition angle denoted by θ depends on three orientation angles indicated as $\boldsymbol{\Phi}$, T_0, and T_1. θ exhibits a linear variation in a characteristic distance denotes as d, and follows the coordinates of the new reference system $'x'$. The notation used to describe the fiber orientation is consistent with that introduced by Gürdal et al. [32] and is detailed in Eq. (1)

$$\theta(x') = \boldsymbol{\Phi} + T_0 + \frac{T_1 - T_0}{d}|x'| \tag{1}$$

where $\boldsymbol{\Phi}$ is the rotation of the local reference system concerning a reference direction. x' is defined from the rotation by the relation $x' = x\cos(\boldsymbol{\Phi}) + y\sin(\boldsymbol{\Phi})$ and the distance d is equal to $a/2$ when $\boldsymbol{\Phi}$ is 0° and equal to $b/2$ when $\boldsymbol{\Phi}$ is 90°. Fig. 1 is included herein to elucidate the fiber deposition process and its associated degrees of freedom.

An example lamination of $[0 < 90, -45 >]$ is represented in Fig. 1, where the fiber orientation is indicated by the use of the three rotation angles. $[0 < 90, -45 >]$ means that $\boldsymbol{\Phi}$ is equal to 0° (and is not reported in the figure), T_0 is equal to 90° and T_1 is −45°. As a consequence, the orientation θ can be calculated replacing the terms in Eq. (1), $x' = x\cos(0) + y\sin(0) = x$ and $\theta(x') = \theta(x) = 0 + 90 + \frac{-45-90}{a/2}|x'| = 90 - \frac{135}{a/2}|x|$.

The material properties are introduced in the structural problem through Hooke law, which links the stress $\boldsymbol{\sigma}$ and the strain $\boldsymbol{\epsilon}$ as reported in Eq. (12). This link is expressed by the material properties matrix $\boldsymbol{C}$ whose explicit formulation can be found in literature [33,34]. $\boldsymbol{C}$ is expressed in the Cartesian global reference system and is obtained from the matrix in the material reference system $\tilde{\boldsymbol{C}}$ from Eq. (2).

$$\boldsymbol{C}(x,y) = \boldsymbol{T}(x,y)\tilde{\boldsymbol{C}}\boldsymbol{T}^T(x,y) \tag{2}$$

Where $\boldsymbol{T}$ is the rotation matrix, and the apex T means transposition. In VAT material, the rotation matrix cannot be uniquely defined, unlike cases with straight fiber configurations. As a result of the continuous variation in the fiber direction, the orientation angle changes from one point to the next, necessitating an alternative formulation for

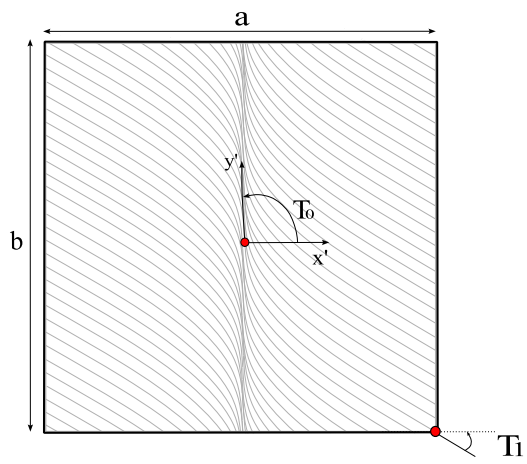

Fig. 1. VAT parameters representation for lamination $[0 < 90, -45 >]$.

describing local material properties. The rotation matrix, denoted as $\boldsymbol{T}(x, y)$, establishes the relationship between the reference system of the element and the reference system of the material. The rotation is a function of the local fiber orientation, which varies across the lamina plane. In commercial software, this issue is addressed by assuming a constant lamination angle throughout the entire finite element domain, which entails increasing the number of elements necessary for an accurate description. Therefore, the present work uses an alternative methodology wherein the VAT material coefficients are calculated in specific Gauss points as outlined by Viglietti et al. [35]. The Gauss point integration approach makes the study of VAT structures more precise and effective by accounting for the variation of the stiffness coefficients of the materials across multiple evaluations in the single finite element.

Usually, the techniques employed to achieve the desired fiber path may exhibit certain imperfections, including misalignment, gap, and overlaps [36,37]. Employing the chosen orientation law, these imperfections in the fiber deposition are not accounted for, and the theoretical deposition is assumed to coincide with the actual deposition, as done in the present work.

3. Mathematical approach to the linearized thermal buckling

3.1. The Carrera Unified Formulation and FEM

The plate theories enable the characterization of structural behavior when at least one dimension is at least one order of magnitude smaller than the in-plane dimensions. A two-dimensional (2D) approach provides a simplified representation of the three-dimensional (3D) structure by introducing established mathematical functions that describe the through-thickness behavior of the primary unknowns in the problem. These primary unknowns are the 3D displacements as detailed in Eq. (3).

$$\boldsymbol{u}^T(x, y, z) = (u, v, w) \tag{3}$$

The complete displacement field can be expressed through a condensed notation provided by the Carrera Unified Formulation. This formulation employs the combination of the expansion functions denoted as $F_\tau(z)$ and the general 2D displacement vector $\boldsymbol{u}_\tau(x, y)$. It lets us schematize the 2D structural problem through an index model that allows the representation of the displacement field as reported in Eq. (4).

$$\boldsymbol{u}(x, y, z) = F_\tau(z)\boldsymbol{u}_\tau(x, y) \qquad \tau = 1, 2, \dots, N \tag{4}$$

Where N is the number of expansion terms, and the double subscript means summation. Within the CUF framework, the formulation remains invariant when the expansion functions $F_\tau(z)$ or their order is changed.

In the present work, two different families of expansion functions will be employed in the formulation, and several kinematic models with different orders are thus employed.

Taylor Expansion functions (TE) are hierarchical polynomials in the thickness coordinate z. TE allows the structural problem to be solved by returning the three-variable dependence unknown to a reference surface, typically the middle one. For instance, Eq. (5) reports a second-order Taylor model. Higher orders of expansion can be achieved by adding terms to the displacement field in a hierarchical progression [31].

$$\begin{cases} u(x, y, z) & = u_0(x, y) \;\|\; + u_1(x, y) \cdot z \;\|\; + u_2(x, y) \cdot z^2 \\ v(x, y, z) & = v_0(x, y) \;\|\; + v_1(x, y) \cdot z \;\|\; + v_2(x, y) \cdot z^2 \\ w(x, y, z) & = \underbrace{w_0(x, y)}_{N=0} \;\|\; \underbrace{+ w_1(x, y) \cdot z}_{N=1} \;\|\; \underbrace{+ w_2(x, y) \cdot z^2}_{N=2} \end{cases} \tag{5}$$

Here, the symbol N denotes the expansion order, and the subscript distinguishes the different coefficients. Taylor models are based on the calculation of displacement values upon a reference surface. High-order terms are particularly desirable in the case of thick plates and composite laminates when classical theories cannot fulfill the Interlaminar Continuity condition C_0^z requirements [38]. Using the Taylor functions, the model is denoted here by TEn, where n denotes the assumed expansion order; the Lagrangian models are indicated in the same way. The classical First Order Shear Deformation Theory (FSDT) can be considered as a special case of TE1 where u and v are assumed to be linear and w presents only the term corresponding to TE0.

Lagrange Expansions (LE) constitute another group of expansion functions $F_\tau(z)$ commonly used in the context of high-order kinematic theories. In LE models, the variables are defined above the physical surface of the structure and consist of pure displacements, not including high-order variables. As a result, the thickness is divided into several local expansion sub-domains, and the degree of the expansion polynomial depends on the type of Lagrange functions used. For the sake of clarity, an example expansion of the third order is reported in Eq. (6).

$$\begin{cases} u(x, y, z) & = u_1(x, y) \cdot F_1(z) + u_2(x, y) \cdot F_2(z) + u_3(x, y) \cdot F_3(z) + u_4(x, y) \cdot F_4(z) \\ v(x, y, z) & = v_1(x, y) \cdot F_1(z) + v_2(x, y) \cdot F_2(z) + v_3(x, y) \cdot F_3(z) + v_4(x, y) \cdot F_4(z) \\ w(x, y, z) & = w_1(x, y) \cdot F_1(z) + w_2(x, y) \cdot F_2(z) + w_3(x, y) \cdot F_3(z) + w_4(x, y) \cdot F_4(z) \end{cases} \tag{6}$$

Usually, to describe the Lagrange functions, it is preferred to use a natural reference system where the variable ξ is defined between -1 and 1. Eq. (7) reports the Lagrange functions related to the third-order expansion.

$$\begin{cases} F_1(z) = -\dfrac{9}{16}\left(\xi + \dfrac{1}{3}\right)\left(\xi - \dfrac{1}{3}\right)(\xi - 1) & \xi_1 = -1 \\ F_2(z) = \dfrac{27}{16}(\xi - 1)\left(\xi - \dfrac{1}{3}\right)(\xi + 1) & \xi_2 = -\dfrac{1}{3} \\ F_3(z) = -\dfrac{27}{16}(\xi + 1)\left(\xi + \dfrac{1}{3}\right)(\xi - 1) & \xi_3 = \dfrac{1}{3} \\ F_4(z) = \dfrac{9}{16}\left(\xi + \dfrac{1}{3}\right)\left(\xi - \dfrac{1}{3}\right)(\xi + 1) & \xi_4 = 1 \end{cases} \tag{7}$$

The CUF power can be fully employed using the FEM within its framework; the FEM approximates the plane unknowns $\boldsymbol{u}_\tau(x, y)$ using two-dimensional shape functions denoted by $N_i(x, y)$. Introducing the FEM in Eq. (4), it is possible to express the displacement in the following form:

$$\boldsymbol{u}(x, y, z) = F_\tau(z)N_i(x, y)\boldsymbol{q}_{\tau i} \tag{8}$$

where $\boldsymbol{q}_{\tau i}$ denotes the nodal displacement, and the (x, y) dependency is transferred from the 2D displacement vector to the shape functions N_i. The order of the finite element changes depending on the number of nodes employed. In the case of a nine-node plate element, a bi-quadratic behavior of the 2D displacement can be characterized. Fig. 2

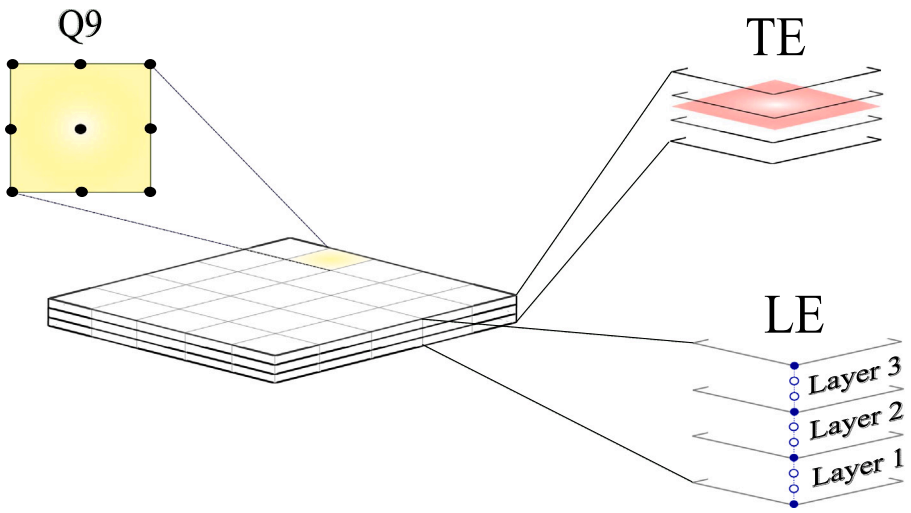

Fig. 2. Nine node finite element disposition (denotes as Q9 in the figure). Third-order Lagrange Expansion (LE) and Taylor Expansion (TE) graphical representation.

depicts the nine nodes finite element distribution, and the TE and LE approaches to modeling through the thickness. In the Taylor model, the reference surface is depicted in red, while Lagrange nodes along the thickness are reported in blue.

Besides the adopted expansion theory, a comprehensive description of the material properties along the thickness becomes imperative, whereas the presence of multi-layers. In the present work, TE models characterize stacking sequences using an ESL approach. Conversely, a LW approach is employed within the Lagrange in-thickness expansion.

The ESL approach involves a description along the thickness in which a material of equivalent properties of the selected lamination is considered. In fact, the in-thickness homogenization simply adds the components relative to the different layers to build the stiffness matrix. On the other hand, the LE unknowns merit supplies to impose BC on displacement variables with a simple LW implementation. As a result, the Layer-Wise approach necessitates considering each layer individually with its specific material properties. Interface conditions are enforced through the stiffness matrix assembly, whose dimensions expand with the order of Lagrange expansion. However, it is worth noting that while the LW approach offers increased accuracy compared to ESL models, it also incurs a higher computational cost. Comprehensive explanations and detailed formulations for both theories can be found in [31].

3.2. Thermal-buckling problem

The thermal problem is here expressed in a purely decoupled form, wherein the thermal profile is treated as an external load with a predetermined behavior. As a result, the primary variables of the problem are the displacements, as defined in Eq. (3). This approach is realistic because the thermal profile analyzed here is constant all over the plate, and the accuracy of the analysis is not reduced using the decoupled model. Furthermore, the computational cost is lower than that of the coupled model.

The expressions of strains and stresses are provided respectively in Eqs. (9) and (10).

$$\boldsymbol{\varepsilon}^T = \left(\varepsilon_{xx}, \varepsilon_{yy}, \varepsilon_{zz}, \varepsilon_{xz}, \varepsilon_{yz}, \varepsilon_{xy}\right) \tag{9}$$

$$\boldsymbol{\sigma}^T = \left(\sigma_{xx}, \sigma_{yy}, \sigma_{zz}, \sigma_{xz}, \sigma_{yz}, \sigma_{xy}\right) \tag{10}$$

The geometrical relations establish the link between strains and displacements via a differential operator denoted as $\boldsymbol{b}$, which explicit form is expressed in Appendix A. The geometrical relations are expressed as follows:

$$\boldsymbol{\varepsilon} = \boldsymbol{bu} \tag{11}$$

The constitutive relation establishes the strain-stress link using the global material properties matrix $\boldsymbol{C}$ whose explicit formulation can be found in [33,34]. It is noteworthy that, in the case of VAT lamina, matrix $\boldsymbol{C}$ becomes a function of the position, $\boldsymbol{C}(x, y)$, implying the action of the differential operator on it. The constitutive equation is presented in Eq. (12) where the material properties matrix is referred to the global reference system and indicates by $\boldsymbol{C}(x, y)$. Additional details can be found in [29] for further insights into the applied rotations and their implications.

$$\boldsymbol{\sigma} = \boldsymbol{C}(x, y)\boldsymbol{\varepsilon} \tag{12}$$

In the decoupled thermo-elastic problem, it is worthwhile to decompose strains and stresses in mechanical and thermal contributions, represented respectively by the subscripts m and ϑ.

$$\boldsymbol{\varepsilon} = \boldsymbol{\varepsilon}_m + \boldsymbol{\varepsilon}_\vartheta \tag{13}$$

$$\boldsymbol{\sigma} = \boldsymbol{C\varepsilon} = \boldsymbol{C}\left(\boldsymbol{\varepsilon}_m + \boldsymbol{\varepsilon}_\vartheta\right) = \boldsymbol{\sigma}_m - \boldsymbol{\beta}\Delta\mathcal{T} \tag{14}$$

Where $\Delta\mathcal{T}$ is the applied over-temperature, $\boldsymbol{\alpha}$ denotes the vector of the coefficients of thermal expansion, and $\boldsymbol{\beta}$ couples the thermal and the mechanical fields and is defined as $\boldsymbol{\beta} = \boldsymbol{C\alpha}$, expressed in the global reference system. It should be noted that the materials properties are considered temperature-independent in the present work.

The non-linear static equilibrium equations can be easily obtained through the Principle of Virtual Displacements (PVD), whose formulation is reported in Eq. (15).

$$\delta L_{int} = \delta L_{ext} \tag{15}$$

Where δL_{int} is the variation of the internal strain energy and δL_{ext} is the variation of the mechanical external load, which is null because no mechanical load is applied. The relation becomes as follows:

$$\delta L_{int} = \int_V \delta\boldsymbol{\varepsilon}^T \boldsymbol{\sigma} dV = \int_V \left(\delta\boldsymbol{\varepsilon}_{\boldsymbol{m}} + \cancel{\delta\boldsymbol{\varepsilon}_\theta}\right)^T \boldsymbol{\sigma} dV = \int_V \delta\boldsymbol{\varepsilon}_{\boldsymbol{m}}^T \boldsymbol{\sigma} dV \tag{16}$$

where the thermal strain is linear with respect to $\boldsymbol{u}$ and the corresponding virtual variation $\delta\boldsymbol{\varepsilon}_\theta$ is zero.

In the context of the decoupled thermal problem, thermal strains are introduced without constituting an unknown of the problem and, consequently, are expressed into the problem within the internal strain energy. Details on the thermally coupled approach and its difference from the decoupled one can be found in [39,40].

The virtual variation of the strain energy is rewritten using Eqs. (8), (11) and, (12). In a compact form, it becomes:

$$\delta L_{int} = \delta \boldsymbol{q}_{sj}^{T} \boldsymbol{K}^{ij\tau s} \boldsymbol{q}_{\tau i} = 0 \tag{17}$$

where through the indices i, j, τ, s the tangent stiffness matrix is expressed in terms of a 3×3 Fundamental Nuclei (FN), and the specific details of the assembling procedure to obtain the matrix $\boldsymbol{K}$ are elucidated in [31]. The stiffness matrix for the entire structure can be computed employing its fundamental components: the FN matrices, which are independent of the selected expansion theory. Four building loops are employed to combine the FN reported in Eq. (17) with the aim of constructing the complete stiffness matrix.

The linearized buckling equations are derived using a linear stability analysis of an undeformed equilibrium configuration, where the critical condition is determined by a proportionally scaled load combined with a geometric or initial stress stiffness resulting from geometric nonlinearities [41]. The following assumptions are introduced: the pre-buckling state is stable, and the initial thermal stress $\boldsymbol{\sigma}^{\circ}$ remains constant and does not vary in magnitude or direction during buckling. The last assumption is that the equilibrium states are infinitesimally adjacent at the bifurcation so that linearization becomes possible. Following these assumptions, the critical load can be defined by a linear relation with the initial stress $\boldsymbol{\sigma}^{\circ}$. Considering the scalar load factor λ, the critical load is $\boldsymbol{\sigma} = \lambda \boldsymbol{\sigma}^{\circ}$, for which a non-trivial solution $\boldsymbol{q} \neq 0$ exists, this is an eigenvalue problem, expressed as follows:

$$\delta \boldsymbol{q}^{T} \; : \quad \left[\boldsymbol{K} + \lambda \boldsymbol{K}_{\sigma}\right] \delta \boldsymbol{q} = 0 \tag{18}$$

where $\boldsymbol{K}$ is the usual linear stiffness matrix from Eq. (17) and $\boldsymbol{K}_{\sigma}$ is the geometric stiffness matrix that is obtained from the expression of the variation of the work done by the virtual non-linear strains with the thermal initial stresses.

$$\int_{V} \delta^{2} \boldsymbol{\varepsilon}_{nl}^{T} \boldsymbol{\sigma} dV \tag{19}$$

Due to the inherent instability associated with the buckling phenomenon, it is necessary to consider the non-linear component of the strain. It is possible to categorize the strain in linear and non-linear vectors where $\boldsymbol{\varepsilon}_{nl}$ is obtained from the non-linear geometrical relations as follows:

$$\boldsymbol{\varepsilon}_{nl} = \boldsymbol{b}_{nl} \boldsymbol{u} \tag{20}$$

where the non-linear terms of the geometrical relations are categorized into the operator $\boldsymbol{b}_{nl}$ whose explicit form is reported in Appendix A. Substituting Eqs. (8) and (20) into Eq. (19) it is possible to obtain the following expression:

$$\begin{aligned} \delta \boldsymbol{q}_{sj}^{T} \int_{V} diag\left[\left(\boldsymbol{B}_{nl}^{*}\right)^{T} \boldsymbol{\sigma}\right] \delta \boldsymbol{q}_{\tau i} dV &= \delta \boldsymbol{q}_{sj}^{T} \int_{V} diag\left[\left(\boldsymbol{B}_{nl}^{*}\right)^{T} \lambda \boldsymbol{\sigma}^{0}\right] \delta \boldsymbol{q}_{\tau i} dV \\ &= \delta \boldsymbol{q}_{sj}^{T} \lambda \boldsymbol{K}_{\sigma}^{ij\tau s} \delta \boldsymbol{q}_{\tau i} \end{aligned} \tag{21}$$

where due to the linearization, it is possible to apply the relation $\boldsymbol{\sigma} = \lambda \boldsymbol{\sigma}^{0}$. The matrix $\boldsymbol{B}_{nl}^{*}$ is obtained by applying the non linear differential operator $\boldsymbol{b}_{nl}$ on the shape functions $N_i(x, y)$ and $N_j(x, y)$ and on the expansion functions $F_{\tau}(z)$ and $F_s(z)$. Its explicit form is expressed in Appendix B; more details are available in [42].

It possible to determine the critical load value, as outlined in Eq. (22).

$$\left|\boldsymbol{K} + \lambda \boldsymbol{K}_{\sigma}\right| = 0 \tag{22}$$

Where the symbol $|\cdot|$ indicates the determinant of the eigenvalue problem. The applied thermal load is indicated by $\Delta\mathcal{T}$, the over-temperature to which the plate is subjected. The critical thermal load will be $\lambda \cdot \Delta\mathcal{T}$ in this linearized scenario.

4. Numerical results

In this section, comprehensive analyses of convergence and sensitivity are presented. Bi-quadratic nine-node finite elements are employed for the in-plane discretization, and high-order theories are used to describe the in-thickness behavior of the multilayer. The results are compared to the relevant literature sources [19,20,30]. Different geometry, materials, and constraints are addressed herein. Furthermore, the influence of the edge-to-thickness ratio and lamination of the plate are investigated, evaluating the best numerical model for each configuration. The following analyses are outlined:

- In Section 4.1, several thermal buckling analyses are conducted on simply supported, square plates of high/modulus Graphite/Epoxy. The adopted material properties are detailed in the following text. Considerations encompass antisymmetric laminations of $[\pm 0 < 15, 15 >]_4$, and $[\pm 0 < 15, 45 >]_4$ with thickness to edge ratios L/h equal to 40 and 10 for each lamination.
- In Section 4.2 there are presented some thermal buckling analyses of simply supported thin symmetric plates composed of Carbon/Epoxy whose properties are listed in Table 7. Lamination considered are $[\pm 0 < 45, 45 >]_s$ and $[\pm 0 < 69, -5.705 >]_s$.
- Section 4.3 collects some results of thermal buckling for the same square VAT plate of the previous section with clamped constraints.
- Section 4.4 collects the results of thermal buckling analyses of simply supported and clamped symmetric square plates as the lamination parameters T_0 and T_1 change.
- In Section 4.5, the influence of different materials on the thermal buckling of the simply supported square plate is investigated. The adopted laminations are taken from [20] and coincide with their found best lamination retarding thermal buckling.

4.1. Simply supported thin and thick plates

The following analyses are carried out on a square plate whose lamination and dimensions are varied to investigate their influence on the evaluation of the buckling critical load. In particular, different ratios between edges and thickness are considered to evaluate their effect on the convergence of the model. Each edge of the square plate is assumed to be subjected to simply support conditions.

Two anti-symmetric stacking sequences, each composed of 8 layers, are considered. The thickness of the plate remains constant at 1 mm, and the edge lengths are changed. The first staking sequence implemented as $[\pm 0 < 15, 15 >]_4$ represents a straight fiber configuration, while the second stacking sequence is $[\pm 0 < 15, 45 >]_4$. It should be noted that the laminations are angle-ply anti-symmetric. Two different geometrical configurations are analyzed with edge-to-thickness ratios L/h equal to 40 and 10 for each plate. A constant one-degree over-temperature $\Delta\mathcal{T} = 1^{\circ}$ C is applied. The material properties present a typical high modulus Graphite/Epoxy: $E_1/E_2 = 40.0$, $E_2 = E_3$, $\nu_{12} = \nu_{13} = \nu_{23} = 0.25$, $G_{12}/E_2 = 0.6$, $G_{12} = G_{13}$, $G_{23}/E_2 = 0.5$, $\alpha_{11} = 1\text{x}10^{-6}$ C^{-1}, $\alpha_{22}/\alpha_{11} = 2$, $E_2 = 10$ GPa. The results in terms of non-dimensional critical temperature are reported in Table 1 and Table 2.

Table 1 displays the results of a convergence analysis where the number of the bi-quadratic plate elements, denoted as Q9, is systematically varied. The purpose of the analysis is to investigate the impact of lamination and thickness ratio on the in-plane discretization. Particular emphasis is given to the difference between the convergence rate of the thick and the moderately thick plates. Table 1 presents the results and compares them to the solutions obtained through Abaqus 2D by Vescovini et al. [30]. The convergence analysis is conducted with TE3 expansion theory that allows good accuracy with a kinematic agreement to the shell ABAQUS 2D model.

Fig. 3 shows the first buckling mode of the plate with both the laminations. The two cases present the same buckling mode with one central main deflection. However, the deflection of the VAT plate is more elliptical.

The results presented in Table 1 show that the method outlined in the present study exhibits a rapid convergence for both the considered

Table 1
Convergence analysis considering the non-dimensional buckling critical temperature $\lambda\alpha_{11} \times 10^3$, using expansion theory TE3 for a simply supported plate made of high modulus Graphite/Epoxy.

		$[\pm 0 < 15, 15 >]_4$		$[\pm 0 < 15, 45 >]_4$		DOFs
		$L/h = 40$	$L/h = 10$	$L/h = 40$	$L/h = 10$	
		$\lambda\alpha_{11} \times 10^3$				
	Abaqus S4R [30]	0.5970	5.9392	0.9769	9.0297	–
	Number of elements [Q9]					
TE3	2 × 2	0.6642	6.9541	1.0372	9.2871	300
	5 × 5	0.6240	6.9710	0.9608	9.2733	1452
	8 × 8	0.6243	7.0297	0.9552	9.4578	3468
	10 × 10	0.6248	7.0532	0.9563	9.5227	5292
	12 × 12	0.6254	7.0669	0.9584	9.5603	7500
	20 × 20	0.6273	7.0794	0.9676	9.6026	20 172

(a) (b)

Fig. 3. First buckling mode for (a) L/h =10, $[\pm 0 < 15, 15 >]_4$, (b) L/h =10, $[\pm 0 < 15, 45 >]_4$, with 10 × 10 Q9.

laminations. Although, the results of the plate with an edge-to-thickness ratio equal to $L/h = 40$ are closer to those taken as reference. Furthermore, they present a more rapid convergence trend than the plate with $L/h = 10$. Conversely, when the plate with a side-to-thickness ratio of 10 is examined, the results deviate slightly from the reference results. In fact, unlike the classical shell model, the method used here accurately considers the effects of shear stress without necessitating any correction factors. A study on the influence of expansion theory is mandatory to investigate the phenomenon deeply.

In the case of the $[\pm 0 < 15, 45 >]_4$, the difference with respect to the published results can also be attributed to the continuous variation in fiber orientation that leads to a problematic description of the material properties. Commercial codes often assume the fiber orientation constant throughout the single element. This assumption can lead to significant approximations in the orientation assessment of VAT. In contrast, the present model evaluates the material properties in each Gauss point, resulting in a more accurate assessment of the results.

Table 2 shows the outcomes of the analyses conducted using different expansion models. The results in Table 2 are compared to the one by Manickam et al. [19] and to the Ritz solution by Vescovini et al. [30]. Manickam et al. [19] derived their solution employing a FSDT with a shear correcting factor of 5/6 and in-plane Q8 elements. Moreover, Vescovini et al. [30] analyses employed the Ritz method with 14 approximation functions and expansion theory equal to the LE2 expansion theory (according to the present notation).

The LE results reported in Table 2 are obtained with a simply supported constraint modeled through a rigid constraining frame. This modelization ensures a good kinematic representation of the constraint that coincides with the one usually used on moderately thick plates.

The results in Table 2 present a good agreement with the references with the TE1 model that provides the same results as the reference. On the other hand, increasing the accuracy of the model, it seems that high-order models provide different results. This difference is due to

Table 2
Expansion theory influence investigation with 10 × 10 Q9 of simply supported plate made of high modulus Graphite/Epoxy reporting non-dimensional buckling temperature $\lambda\alpha_{11} \times 10^3$.

	$[\pm 0 < 15, 15 >]_4$		$[\pm 0 < 15, 45 >]_4$		DOFs
	$L/h = 40$	$L/h = 10$	$L/h = 40$	$L/h = 10$	
	$\lambda\alpha_{11} \times 10^3$				
TE1	0.5996	5.9244	0.9412	8.3836	2646
TE3	0.6248	7.0532	0.9563	9.5227	5292
LE2	0.6905	7.6585	0.8792	8.8819	22 491
LE3	0.6906	7.7440	0.8793	8.9355	33 075
Ref. [19]	0.6010	6.2184	1.0131	9.5633	–
Ref. [30]	0.6018	6.0010	0.9782	8.7768	–

the combination of the volumetric effect of the thermal load and the high anisotropy presented in the laminates that cannot be described through lower-order theories. The major difference between LE3 and TE1 is observed in the plate with $[\pm 0 < 15, 15 >]_4$ and $L/h = 10$. As expected, increasing the edge-to-thickness ratio reduces this difference. Furthermore, the plate with straight fiber presents higher anisotropy than the correspondent VAT plate.

Fig. 4 shows the mechanical and thermal anisotropy for the plate with lamination $[0 < 15, 45 >]$ and $[0 < 15, 15 >]$, which represent the first ply of each plate. It is clear, from the fiber path depicted on the plate illustration, that the anisotropies of both laminations are reported side to side. In the plate with straight fiber deposition, the anisotropies are constant all over the plate. On the other hand, the anisotropies of the VAT plate are observed to be symmetric to the y axis with a variation along the x axis. The fiber direction that leads to higher anisotropy is $\alpha = 15°$ for both cases. This result means that the straight-fiber plate possesses a higher value of anisotropy. For this reason, the high-order theories have a higher impact on the outcomes, allowing

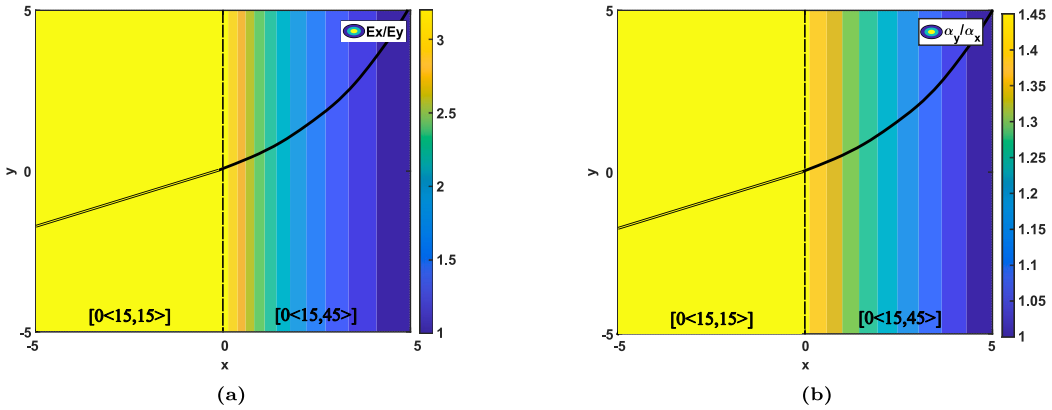

Fig. 4. Mechanical (a) and thermal (b) anisotropy for different fiber orientations of the $L/h = 10$ plate.

Table 3
Convergence analysis considering buckling critical temperature $\Delta\mathcal{T}$, using one LE3 for each layer for a simply supported Carbon/Epoxy plate.

Lamination	$[\pm 0 < 45, 45 >]_s$	$[\pm 0 < 69, -5.705 >]_s$	
Number of elements [Q9]	Critical temperature [°C]		DOFs
10 × 10	42.76	59.02	17 199
16 × 16	42.34	57.59	42 471
20 × 20	42.25	57.43	65 559
24 × 24	42.22	57.45	93 636
References [20]			
20 × 20 [Q4]	42.21	57.79	–

Table 4
Expansion theory influence investigation with 20 x 20 Q9 of simply supported Carbon/Epoxy plate reporting the buckling critical temperature.

Lamination	$\Delta\mathcal{T}_{cr}$					
	TE1	TE2	TE3	LE2	LE3	Refs. [20]
$[\pm 0 < 45, 45 >]_s$	42.82	42.00	41.88	42.25	42.25	42.21
$[\pm 0 < 69, -5.705 >]_s$	58.17	56.55	56.47	57.43	57.43	57.79
DOFs	10 087	15 129	20 172	45 387	65 559	–

a better description of the out-of-plane phenomena. Moreover, these phenomena are further enhanced for the thick plates.

The influence of the curved fiber is more significant in the in-plane convergence. On the other hand, volumetric effect and anisotropy are more critical in choosing the expansion theory. Notably, TE1 yields results that are very close to the 2D reference model. However, due to the edge-to-thickness ratio, the plate is not thin. For this reason, the LE model is necessary in each case to ensure good results.

4.2. Symmetric simply supported plate

The following analysis is conducted on the square plate presented by Duran et al. [20], who have provided a comprehensive set of buckling results for different materials. The first analysis focuses on the thermal buckling of a Carbon/Epoxy simply supported square plate with different laminations. The selected laminations include $[\pm 0 < 45, 45 >]_s$ and the optimal lamination provided by Duran et al. [20]. The choice of $[\pm 0 < 45, 45 >]_s$ aims to attain the maximum buckling critical temperature that can be obtained through classical lamination, as demonstrated in existing literature [43]. Furthermore, these results are then compared with VAT ones to the $[\pm 0 < 69, -5.705 >]_s$ lamination. A sensitivity analysis of the adopted expansion theory is presented to determine the most suitable order for accurately characterizing the critical buckling thermal load.

The subsequent analyses focus on a four-layer square plate with an edge of 150 mm and a thickness of 1.016 mm. The external load is a constant one-degree over-temperature across the whole plate. Moreover, the orientation of the first ply of each lamination is illustrated in Fig. 5. The material that composes the plate is Carbon/Epoxy, whose properties are taken from [20] and are reported in Table 7.

Table 3 provides numerical values derived from the convergence analysis for the different laminations. This convergence analysis entails using Q9 elements with LE3 expansion function. In Table 3, reference results are reported from [20], which model is based on four-node FEM Kirchhoff elements, adequate to represent the thin plates.

From the results in Table 3, it becomes evident that a 16 × 16 discretization yields results comparable to the reference. However, considering all the reported results, a 20 × 20 Q9 mesh is selected for the following analyses to enhance result accuracy.

Due to the thickness of the plate, which is very thin, the main difference in the convergence trend between the straight fiber lamination and the VAT deposition is the introduced approximation of the fiber orientation. This approximation is done in the Gauss points as clarified in Section 2. It implies that the present formulation provides a more accurate evaluation of the VAT fiber orientation with more rapid in-plane convergence with respect to commercial codes. For this reason, the VAT model presents a more rapid convergence of the results to the reference results. As a consequence, in the straight-fiber lamination plate, there is no significant increase in convergence rate compared to the reference.

The influence of the order of the in-thickness expansion theory is now reported in Table 4. The same results are shown in Fig. 5, where bar diagrams represent the buckling critical temperatures obtained through different high-order theories. These results are compared to the reference by Duran et al. [20].

The ratio of the edge to the thickness of the plate is approximately 148, which results in a negligible effect of the expansion theory in terms of the description of the shear effect. On the other hand, the TE and LE models do not exhibit a uniform convergence trend. This is due to the kinematic model which allows distinct description of the volumetric effect. In the LE models, the in-thickness discretization, consisting of physical nodes along the thickness, provides wider freedom for the volumetric effect of the thermal load. However, it is necessary to use LE models to achieve good results when introducing VAT laminated plates, as shown in Fig. 5. Therefore, the LE2 and LE3 models provide identical results, in contrast to the findings presented in Section 4.1, where the thickness effect also determines the choice of theory.

4.3. Symmetric clamped plate

In the following subsection, the analyses are focused on a plate whose geometry, external loading conditions, and material remain consistent with the previous analysis (Section 4.2). The difference is in

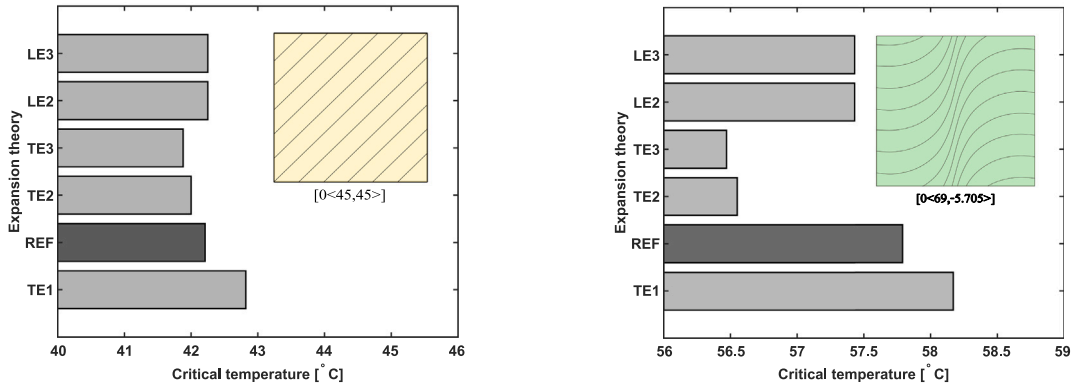

Fig. 5. Buckling critical temperature depending on the expansion theory with 20 × 20 Q9 of a simply supported plate made of Carbon/Epoxy. Lamination $[\pm 0 < 45, 45 >]_s$ (a), $[\pm 0 < 69, -5.705 >]_s$ (b).

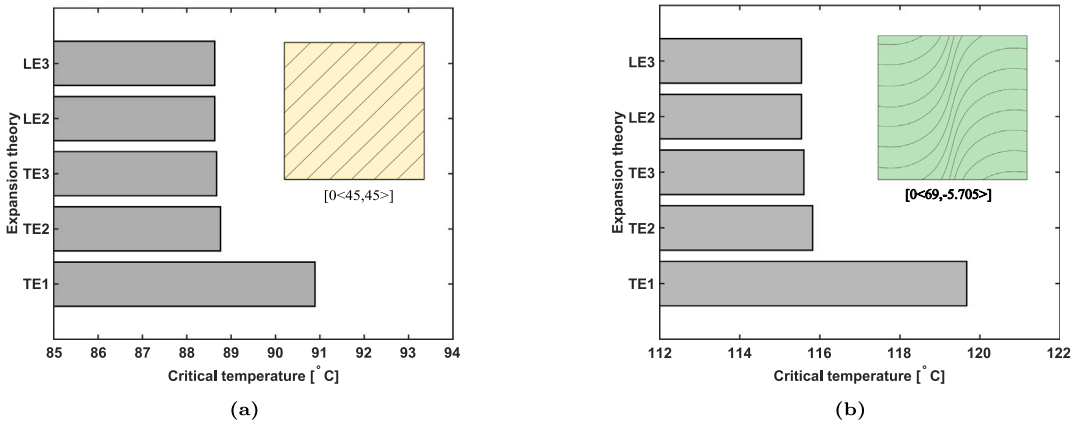

Fig. 6. Buckling critical temperature depending on the expansion theory with 20 × 20 Q9 of a clamped plate made of Carbon/Epoxy. Lamination $[\pm 0 < 45, 45 >]_s$ (a), $[\pm 0 < 69, -5.705 >]_s$ (b).

Table 5
Expansion theory influence investigation with 20 x 20 Q9 of clamped Carbon/Epoxy plate reporting the buckling critical temperature.

Lamination	ΔT_{cr}				
	TE1	TE2	TE3	LE2	LE3
$[\pm 0 < 45, 45 >]_s$	90.89	88.76	88.67	88.63	88.63
$[\pm 0 < 69, -5.705 >]_s$	119.67	115.82	115.60	115.54	115.54
DOFs	10 087	15 129	20 172	45 387	65 559

the constraint conditions with edges of the plate that are fully clamped. Therefore, the influence of the variation in boundary conditions is investigated. Emphasis is given to the expansion theory choice and to the buckling critical temperature changes. The results are collected in Table 5 and in Fig. 6. The Figure presents two bar diagrams collecting the critical temperature obtained through different models for lamination of $[0 < 45, 45 >]$, and $[0 < 69, -5.705 >]$.

The results show that, in the case of thin clamped plates, as opposed to a simply supported one, all the models with orders higher than TE1 produce comparable outcomes. As a result, in both straight fiber and VAT laminations, opting for TE2 would sufficiently assure high-quality results whilst simultaneously reducing the computational cost compared to LE. Furthermore, as expected, the critical temperature of a clamped plate increases to the simply supported case. It must be noted that when the plate presents all edges clamped, the critical temperature converges consistently in both kinematic models, with a single decreasing trend. In fact, by clamping the entire thickness of the plate, there is no longer any volumetric edge effect due to the model adopted.

4.4. Effect of the orientation parameters

The same plate is analyzed hereafter, changing the lamination parameters. Geometry and external load are consistent with the last considered plate.

Figs. 8 and 9 show the different iso-temperature distributions achieved by changing the orientation parameters while maintaining specific plate constraints. These constraints are imposed on both lamination and boundary conditions, as depicted in Fig. 7.

The results reported in Fig. 8 are conducted on a simply supported plate, and the stacking sequence is held constant to $[\pm\theta]_s$. A plate with the same lamination, material and geometry and with the clamped edge is analyzed, and the relative iso-temperature distributions are reported in Fig. 9.

The parameter Φ is held at a fixed angle of 0°, and both T_0 and T_1 have been changed from −90° to 90° to represent how the critical temperature changes depending on the fiber orientation of the Carbon/Epoxy square plate. The most effective lamination for increasing the critical buckling temperature has been determined by applying various expansion theories. Furthermore, these analyses allow the description of the influence of the lamination and of the constraint on the critical temperature.

Figs. 8 and 9 present iso-temperature surfaces, illustrating the outcomes obtained using various expansion theories. Due to the results

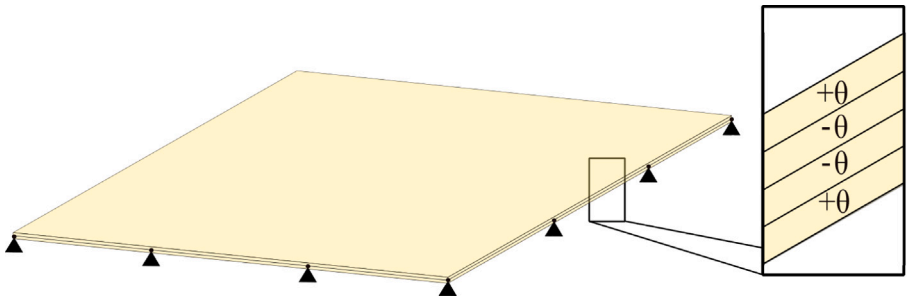

Fig. 7. Plate simply supported and lamination constraints.

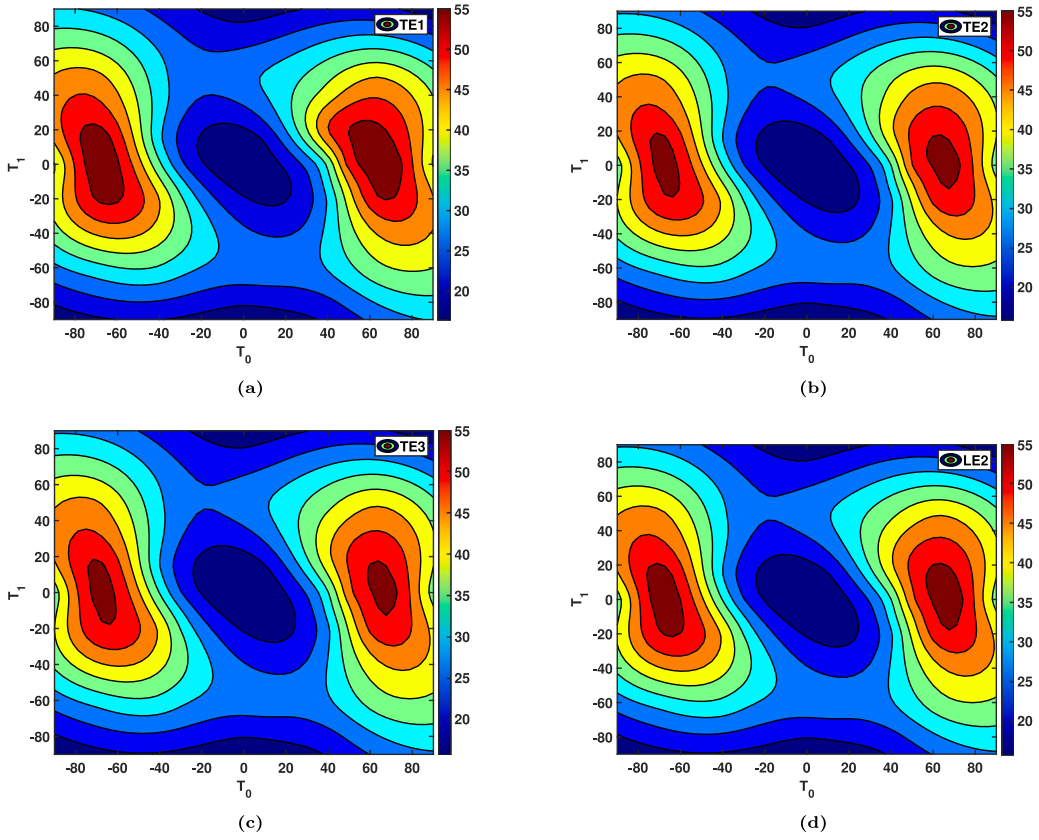

Fig. 8. Critical temperature changing the lamination parameters T_0 and T_1 obtained through the different expansion theories with 20 × 20 Q9, for simply supported Carbon/Epoxy plate. TE1 (a), TE2 (b), TE3 (c), LE2 (d).

Table 6
Influence of the expansion theory on determining the maximum critical temperature and corresponding lamination for simply supported and clamped plate made of Carbon/Epoxy.

Expansion theory	TE1	TE2	TE3	LE2	Ref. [20]
			Simply Supported		
Best staking sequence	$[\pm 0 < 68.3, -0.45 >]_s$				$[\pm 0 < 69, -5.705 >]_s$
Critical temperature [C°]	58.42	56.82	56.73	57.76	57.79
			Clamped		
Best staking sequence	$[\pm 0 < 65.3, -17.75 >]_s$				–
Critical temperature [C°]	128.19	124.47	124.27	124.22	–

obtained in Section 4.2 and Section 4.3 where LE2 and LE3 models gave the same outcomes, the LE3 model is not used in the present analyses.

Notably, TE1 models result in a contour plot depicting a zone of lamination that allows for the higher temperatures. In the simply supported plate, LE models are not represented in a monotonous trend with TE models, as instead, it happens in the clamped plate. However, there is a great variability on reachable maximum critical temperature, which strongly depend on the fiber orientation.

The clamped configurations allow for a higher critical temperature with respect to the simply supported constraint. Furthermore, the

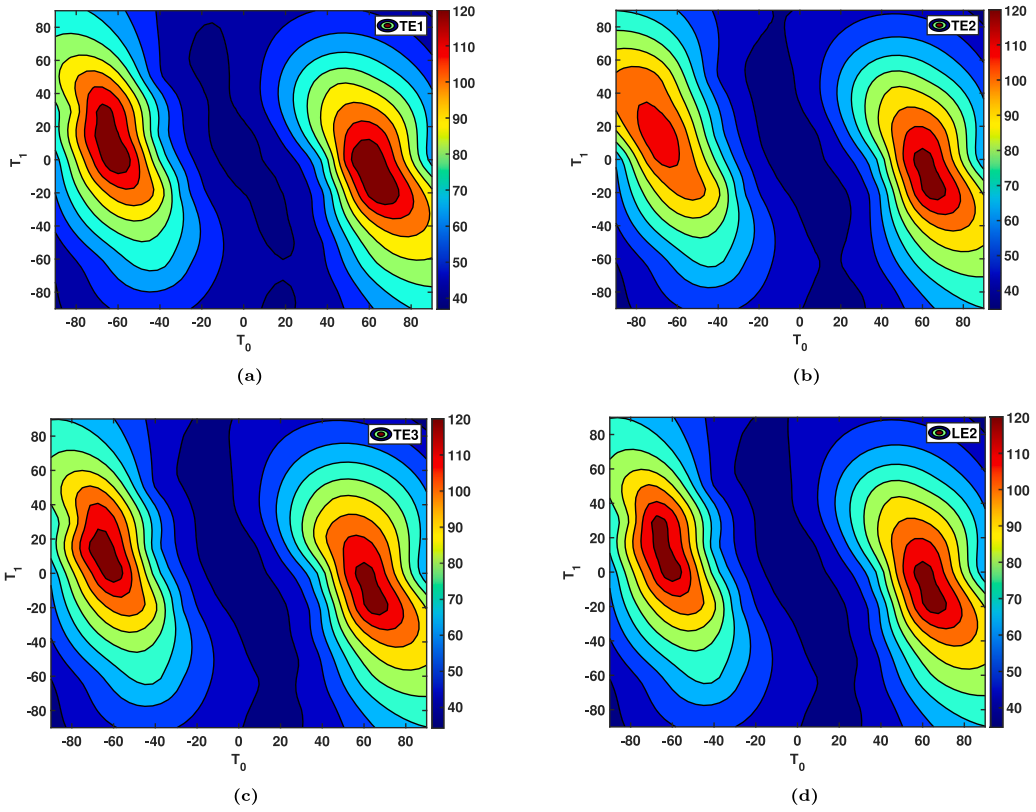

Fig. 9. Critical temperature changing the lamination parameters T_0 and T_1 obtained through the different expansion theories with 20 × 20 Q9, for clamped Carbon/Epoxy plate. TE1 (a), TE2 (b), TE3 (c), LE2 (d).

Table 7
Material properties: mechanical properties [GPa], thermal properties $C°$ x 10^{-6}.

Material	E_1	$E_2 = E_3$	$\nu_{12} = \nu_{13}$	ν_{23}	$G_{12} = G_{13}$	G_{23}	α_{11}	$\alpha_{22} = \alpha_{33}$
Graphite/Epoxy	155	8.07	0.22	0.22	4.55	3.90	−0.07	30.1
E-Glass/Epoxy	41	10.04	0.28	0.28	4.3	3.45	7.0	26
Carbon/Epoxy	147	10.3	0.27	0.27	7.0	5.45	−0.9	27
Kevlar/Epoxy	80	5.5	0.34	0.34	2.2	1.83	−2.0	60
Boron/Epoxy	201	21.7	0.17	0.035	5.4	3.69	6.1	30

dependence of the critical temperature on the lamination parameters shows a different trend between the two constraints configuration.

Table 6 collects the maximum critical temperature values achieved by modifying lamination parameters for each theory. It is evident that the lamination configuration associated with the maximum critical temperature remains consistent across all numerical models, as demonstrated for the mechanical case by Sanchez-Majano and Pagani in [44]. The difference is present in the critical temperature, which changes with the models. Furthermore, with the enhancement of numerical model accuracy, the range of lamination parameters amenable to achieving a substantial increase in critical temperature becomes narrower. The same trend of the results are obtained for the clamped plate.

4.5. Material properties influence

Several analyses are conducted, considering the VAT optimum lamination parameters by Duran et al. [20] for different materials. The mesh utilized is a 20 × 20 Q9, and TE2, LE2 and LE3 expansion theories are compared. Table 7 lists the material properties, while geometry and thermal loading conditions are the same of the previous cases. The constraints applied to the lamination and the boundary conditions are depicted in Fig. 7. The parameter Φ is fixed to 0°, and the selected lamination angles T_0 and T_1 are specified in Table 8.

The results presented in Table 8 demonstrate the effectiveness of the current approach in yielding good outcomes for each analyzed material. As material properties are altered, the choice of the appropriate expansion theory also changes due to the increased benefits of using Lagrange functions in combination with Layer-Wise models in highly anisotropic materials. Fig. 10 shows that the buckling critical temperature strongly depends on the mechanical anisotropy of the material. Furthermore, the use of LE models becomes more necessary with the increase in the anisotropy of the thermal properties of the material as shown in Fig. 10(b), which reports the relative percentage difference of the temperature calculated through the TE2 and LE3 models.

5. Conclusions

The present work addresses thermal buckling problems in which the governing equations are obtained through the Principle of Virtual Displacements (PVD) and the Carrera Unified Formulation (CUF). Furthermore, the thermal problem is schematized via a decoupled representation, and the buckling analyses employ a linearized formulation to obtain the critical temperature through the solution of the eigenvalue problem. The material properties are independent of the applied temperature. A linearized analysis was conducted to calculate the critical buckling load, which coincided with the bifurcation load.

Table 8
Buckling critical temperature ΔT of simply supported plate, lamination constraint $[\pm\theta]_s$ with 20 × 20 Q9, comparing TE2, LE2, LE3 expansion theories.

Material	T_0	T_1	ΔT_{crit}				
			Duran et al. [20]	Vascovini et al. [30]	TE2	LE2	LE3
Graphite/Epoxy	60.70	32.19	34.26	32.96	34.06	34.53	34.53
E-Glass/Epoxy	6.71	58.04	5.58	5.55	5.58	5.60	5.60
Carbon/Epoxy	69.00	−5.705	57.79	–	56.55	57.43	57.43
Kevlar/Epoxy	66.05	11.73	22.18	–	21.54	22.06	22.06
Boron/Epoxy	−6.57	63.28	7.50	7.55	7.43	7.48	7.48

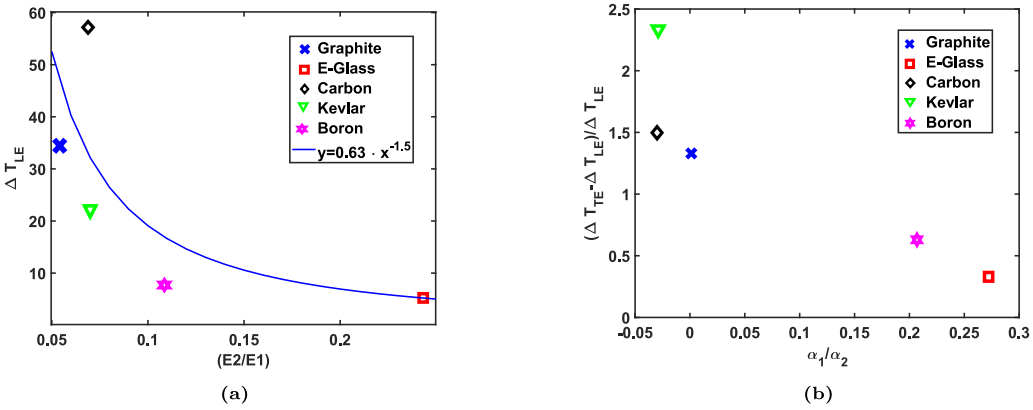

Fig. 10. Temperature and accuracy of the LE model depending on thermal and mechanical anisotropy.

Different geometries, materials, and constraints are analyzed. Furthermore, the ratio-to-edges and the lamination of the plates are changed to evaluate their influence.

Using CUF-based FEM for 3D thermal stress analyses of VAT plates makes it possible to investigate the different shear deformation theories, including ESL and LW. Due to the anisotropy of the composite materials and particularly of the VAT, the investigation of these models becomes interesting for all the studies where the distribution of stresses affects the results, such as the buckling problems. As a consequence of the use of the high-order models, it is possible to describe the stiffness distribution with high fidelity through the thickness and in-plane, building an accurate geometrical stiffness matrix. This is not the case in commercial software simulation, where the stiffness is constant element-wise. The presented results allow for some final considerations:

- As well known, tow-steered fiber allows to retard the critical buckling temperature. The choice of VAT fiber orientation in the plane makes it possible for the critical temperature to be customized over a wide range.
- Due to the high influence of the boundary effect, LE models are preferable for simply supported plates as they provide greater accuracy. Conversely, TE models are accurate enough to describe the critical temperature, reducing the computational cost for the analyses of thin clamped plates.
- The previous point is also justified by the volumetric effects of the thermal load, which is more evident in the case of simply supported constraint, where the edge effects due to the thermal expansion can be more present.
- As the selected expansion theory changes, the parameters T_0 and T_1 of the VAT lamination that allow the maximum critical temperature to be reached remain unchanged in both simply supported and clamped configurations for the considered plate configuration.
- Thermal and mechanical anisotropies influence the choice of the expansion model to adopt; more accurate models are necessary to ensure good results as the anisotropy increases. Furthermore, the edge-to-thickness ratio influences the choice of the better kinematical model; as the plate is thicker, the shear effect is more present, and higher-order theories are preferable.

These analyses gave us accurate and reliable results for the studies of linearized thermal buckling. Future research will deal with geometrically non-linear and post-buckling analysis.

CRediT authorship contribution statement

F. Bracaglia: Writing – original draft, Visualization, Validation, Software, Investigation, Formal analysis. **R. Masia:** Writing – review & editing, Visualization, Software, Investigation, Data curation. **A. Pagani:** Writing – review & editing, Supervision, Resources, Funding acquisition, Conceptualization. **E. Zappino:** Writing – review & editing, Supervision, Software, Methodology, Conceptualization. **E. Carrera:** Writing – review & editing, Supervision, Methodology, Funding acquisition, Conceptualization.

Declaration of competing interest

The authors declare that they have no known competing financial interests or personal relationships that could have appeared to influence the work reported in this paper.

Data availability

Data will be made available on request.

$$\boldsymbol{B}^{*}_{nl} = \begin{bmatrix} F_\tau F_s N_{i,x} N_{j,x} & F_\tau F_s N_{i,x} N_{j,x} & F_\tau F_s N_{i,x} N_{j,x} \\ F_\tau F_s N_{i,y} N_{j,y} & F_\tau F_s N_{i,y} N_{j,y} & F_\tau F_s N_{i,y} N_{j,y} \\ F_{\tau,z} F_{s,z} N_i N_j & F_{\tau,z} F_{s,z} N_i N_j & F_{\tau,z} F_{s,z} N_i N_j \\ F_\tau F_{s,z} N_{i,x} N_j + F_{\tau,z} F_s N_i N_{j,x} & F_\tau F_{s,z} N_{i,x} N_j + F_{\tau,z} F_s N_i N_{j,x} & F_\tau F_{s,z} N_{i,x} N_j + F_{\tau,z} F_s N_i N_{j,x} \\ F_\tau F_{s,z} N_{i,y} N_j + F_{\tau,z} F_s N_i N_{j,y} & F_\tau F_{s,z} N_{i,y} N_j + F_{\tau,z} F_s N_i N_{j,y} & F_\tau F_{s,z} N_{i,y} N_j + F_{\tau,z} F_s N_i N_{j,y} \\ F_\tau F_s N_{i,x} N_{j,y} + F_\tau F_s N_{i,y} N_{j,x} & F_\tau F_s N_{i,x} N_{j,y} + F_\tau F_s N_{i,y} N_{j,x} & F_\tau F_s N_{i,x} N_{j,y} + F_\tau F_s N_{i,y} N_{j,x} \end{bmatrix} \tag{24}$$

Box I.

Acknowledgements

This project has received funding from the European Research Council (ERC) under the European Union's Horizon 2020 research and innovation programme (Grant Agreement No. 850437).

Appendix A. Geometrical relation

$$\boldsymbol{b}_l = \begin{pmatrix} \frac{\partial}{\partial x} & 0 & 0 \\ 0 & \frac{\partial}{\partial y} & 0 \\ 0 & 0 & \frac{\partial}{\partial z} \\ \frac{\partial}{\partial z} & 0 & \frac{\partial}{\partial x} \\ 0 & \frac{\partial}{\partial z} & \frac{\partial}{\partial y} \\ \frac{\partial}{\partial y} & \frac{\partial}{\partial x} & 0 \end{pmatrix} \qquad \boldsymbol{b}_{nl} = \begin{pmatrix} \frac{1}{2}\left(\frac{\partial}{\partial x}\right)^2 & \frac{1}{2}\left(\frac{\partial}{\partial x}\right)^2 & \frac{1}{2}\left(\frac{\partial}{\partial x}\right)^2 \\ \frac{1}{2}\left(\frac{\partial}{\partial y}\right)^2 & \frac{1}{2}\left(\frac{\partial}{\partial y}\right)^2 & \frac{1}{2}\left(\frac{\partial}{\partial y}\right)^2 \\ \frac{1}{2}\left(\frac{\partial}{\partial z}\right)^2 & \frac{1}{2}\left(\frac{\partial}{\partial z}\right)^2 & \frac{1}{2}\left(\frac{\partial}{\partial z}\right)^2 \\ \frac{\partial}{\partial x}\cdot\frac{\partial}{\partial z} & \frac{\partial}{\partial x}\cdot\frac{\partial}{\partial z} & \frac{\partial}{\partial x}\cdot\frac{\partial}{\partial z} \\ \frac{\partial}{\partial y}\cdot\frac{\partial}{\partial z} & \frac{\partial}{\partial y}\cdot\frac{\partial}{\partial z} & \frac{\partial}{\partial y}\cdot\frac{\partial}{\partial z} \\ \frac{\partial}{\partial x}\cdot\frac{\partial}{\partial y} & \frac{\partial}{\partial x}\cdot\frac{\partial}{\partial y} & \frac{\partial}{\partial x}\cdot\frac{\partial}{\partial y} \end{pmatrix} \tag{23}$$

Where the symbol $\partial/\partial(\cdot)$ indicates the partial derivative.

Appendix B. Explicit form of $\mathbf{B}^{*}_{nl}$

The explicit form of the matrix $\boldsymbol{B}^{*}_{nl}$ is reported following employing the CUF notation (see Box I).

References

[1] Tsai S, Massard TN. Composites design, no. ada157710. 1984, Wright-Patterson air force base, Ohio 45433, Final rept..
[2] Peters ST. Handbook of composites. 2nd ed.. Boston, MA: Springer US; 1998.
[3] Kapania RK. A review on the analysis of laminated shells. J Press Vessel Technol 1989;111(2):88–96.
[4] Mangalgiri PD. Composite materials for aerospace applications. Bull Mater Sci 1999;22(3):657–64.
[5] Hyer MW, Charette RF. Use of curvilinear fiber format in composite structure design. AIAA J 1991;29(6):1011–5.
[6] Hyer MW, Lee HH. The use of curvilinear fiber format to improve buckling resistance of composite plates with central circular holes. Compos Struct 1991;18(3):239–61.
[7] Shafighfard T, Demir E, Yildiz M. Design of fiber-reinforced variable-stiffness composites for different open-hole geometries with fiber continuity and curvature constraints. Compos Struct 2019;226:111280.
[8] Pagani A, Azzara R, Carrera E. Geometrically nonlinear analysis and vibration of in-plane-loaded variable angle tow composite plates and shells. Acta Mech 2022;234(1):85–108.
[9] Setoodeh S, Abdalla MM, Jsselmuiden STI, Gürdal Z. Design of variable-stiffness composite panels for maximum buckling load. Compos Struct 2009;87(1):109–17.
[10] Fallahi N, Viglietti A, Carrera E, Pagani A, Zappino E. Effect of fiber orientation path on the buckling, free vibration, and static analyses of variable angle tow panels. Facta Univ Ser: Mech Eng 2020;18(2):165.
[11] Riks E. Buckling. In: Encyclopedia of computational mechanics. 2nd Ed.. Wiley; 2017, p. 1–29.
[12] Gossard ML, Seide P, Roberts WM. Thermal buckling of plates. Techreport 2771, Langley Aeronautical Laboratory Langley Field, Va: NACA; 1952.
[13] Klosner JM, Forray MJ. Buckling of simply supported plates under arbitrary symmetrical temperature distributions. J Aerosp Sci 1958;25(3):181–4.
[14] Whitney JM, J.E. Ashton. Effect of environment on the elastic response of layered composite plates. AIAA J 1971;9(9):1708–13.
[15] Thangaratnam KR, Palaninathan, Ramachandran J. Thermal buckling of composite laminated plates. Comput Struct 1989;32(5):1117–24.
[16] Shiau LC, Kuo SY, Chen CY. Thermal buckling behavior of composite laminated plates. Compos Struct 2010;92(2):508–14.
[17] Chen WJ, Lin PD, Chen LW. Thermal buckling behavior of thick composite laminated plates under nonuniform temperature distribution. Comput Struct 1991;41(4):637–45.
[18] Li F, Nie GJ. Thermo-mechanical buckling analysis of symmetric vat composite laminates with temperature-dependent material properties. Thin-Walled Struct 2019;140:263–71.
[19] Manickam G, Bharath A, Das AN, Chandra A, Barua P. Thermal buckling behaviour of variable stiffness laminated composite plates. Mater Today Commun 2018;16:142–51.
[20] Duran AV, Fasanella NA, Sundararaghavan V, Waas AM. Thermal buckling of composite plates with spatial varying fiber orientations. Compos Struct 2015;124:228–35.
[21] Reddy JN. An evaluation of equivalent-single-layer and layerwise theories of composite laminates. Compos Struct 1993;25(1–4):21–35.
[22] Carrera E, Petrolo M. Guidelines and recommendations to construct theories for metallic and composite plates. AIAA J 2010;48(12):2852–66.
[23] Trabelsi S, Frikha A, Zghal S, Dammak F. Thermal post-buckling analysis of functionally graded material structures using a modified FSDT. Int J Mech Sci 2018;144:74–89.
[24] Trabelsi S, Frikha A, Zghal S, Dammak F. A modified FSDT-based four nodes finite shell element for thermal buckling analysis of functionally graded plates and cylindrical shells. Eng Struct 2019;178:444–59.
[25] Oliveri V, Milazzo A, Weaver PM. Thermo-mechanical post-buckling analysis of variable angle tow composite plate assemblies. Compos Struct 2018;183:620–35.
[26] Liang K, Mu J, Yin Z. Thermoelastic geometrically nonlinear analysis and optimization of variable stiffness composite plates in presence of buckling. Eng Comput 2024.
[27] Chen X, Nie G, Yang X. Thermal postbuckling analysis of variable angle tow composite cylindrical panels. J Therm Stresses 2021;44(7):850–82.
[28] Sánchez-Majano AR, Azzara R, Pagani A, Carrera E. Accurate stress analysis of variable angle tow shells by high-order equivalent-single-layer and layer-wise finite element models. Materials 2021;14(21):6486.
[29] Pagani A, Sanchez-Majano AR. Influence of fiber misalignments on buckling performance of variable stiffness composites using layerwise models and random fields. Mech Adv Mater Struct 2020;29(3):384–99.
[30] Vescovini R, Dozio L. Thermal buckling behaviour of thin and thick variable-stiffness panels. J Compos Sci 2018;2(4):58.
[31] Carrera E, Cinefra M, Petrolo M, Zappino E. Finite element analysis of structures through unified formulation. Chichester, West Sussex, UK: John Wiley & Sons; 2014.
[32] Gürdal Z, Tatting BF, Wu CK. Variable stiffness composite panels: Effects of stiffness variation on the in-plane and buckling response. Composites A 2008;39(5):911–22.
[33] Bathe KJ. Finite element procedures. Bathe, Boston, USA: Bathe, Klaus-Jürgen: Finite element procedures in engineering analysis; 2006, Frühere Ausg. u.d.T..
[34] Hughes TJR. The finite element method. Mineola, NY: Dover Publications; 2000, Reprint. Originally published, Englewood Cliffs, N.J. : Prentice-Hall, 1987,
[35] Viglietti A, Zappino E, Carrera E. Analysis of variable angle tow composites structures using variable kinematic models. Composites B 2019;171:272–83.
[36] Heinecke F, Willberg C. Manufacturing-induced imperfections in composite parts manufactured via automated fiber placement. J Compos Sci 2019;3(2):56.

[37] Pagani A, Sanchez-Majano AR, Zamani D, Petrolo M, Carrera E. Fundamental frequency layer-wise optimization of tow-steered composites considering gaps and overlaps. Aerotecnica Missili Spazio 2024;(212).
[38] Carrera E. CZ° requirements—models for the two dimensional analysis of multilayered structures. Compos Struct 1997;37(3–4):373–83.
[39] Nali P, Carrera E, Calvi A. Advanced fully coupled thermo-mechanical plate elements for multilayered structures subjected to mechanical and thermal loading. Internat J Numer Methods Engrg 2010;85(7):896–919.
[40] Carrera E, Valvano S. A variable kinematic shell formulation applied to thermal stress of laminated structures. J Therm Stresses 2016;40(7):803–27.
[41] Ibrahim SM, Carrera E, Petrolo M, Zappino E. Buckling of composite thin walled beams by refined theory. Compos Struct 2012;94(2):563–70.
[42] Pagani A, Carrera E. Unified formulation of geometrically nonlinear refined beam theories. Mech Adv Mater Struct 2016;25(1):15–31.
[43] Walker M, Reiss T, Adali S, Verijenko VE. Optimal design of symmetrically laminated plates for maximum buckling temperature. J Therm Stresses 1997;20(1):21–33.
[44] Sánchez-Majano AR, Pagani A. Buckling and fundamental frequency optimization of tow-steered composites using layerwise structural models. AIAA J 2023;61(9):4149–63.